J Mater Sci: Mater Med (2011) 22:201–208
DOI 10.1007/s10856-010-4200-8

Synthesis of $CaO–SiO_2–P_2O_5$ mesoporous bioactive glasses with high P_2O_5 content by evaporation induced self assembly process

Shan Zhao · Yanbao Li · Dongxu Li

Received: 29 July 2010 / Accepted: 26 November 2010 / Published online: 14 December 2010

Abstract Mesoporous bioactive glasses (MBGs) of the $CaO–SiO_2–P_2O_5$ system containing relatively high P_2O_5 contents (10–30 mol%) were prepared from a sol–gel. An evaporation-induced self-assembly (EISA) technique was used with poly(ethylene oxide)-block–poly(propylene oxide)-block–poly(ethylene oxide) ($EO_{20}–PO_{70}–EO_{20}$, P123) acting as a template. The structural, morphological and textural properties of MBGs were investigated by small-angle X-ray diffraction (SAXRD), transmission electron microscopy (TEM), Fourier transform infrared (FTIR) spectroscopy and a N_2 sorption/desorption technique. SAXRD and TEM results display the reduced long-range ordering of mesopores with increasing P_2O_5 content. N_2 sorption/desorption analysis shows that all three samples exhibit a type IV isotherm with type H1 hysteresis loops, characteristic of independent cylindrical slim pore channels and this material has a Barret–Joyner–Halenda (BJH) model pore size of $\sim$4 nm and BET specific surface area $\sim$430 m^2/g. NMR results indicate a more condensed framework for samples with 30 mol% P_2O_5 than samples with 10 mol% P_2O_5. For in vitro bioactivity tests where samples were soaked in simulated body fluid (SBF), samples with 30 mol% P_2O_5 showed higher crystallinity than those with lower P_2O_5 contents Silicon concentration increased in SBF solution during the soaking period, which indicates MBGs can be degradable in SBF solution.

S. Zhao · Y. Li (✉) · D. Li (✉)
State Key Laboratory of Materials-Oriented Chemical Engineering, College of Materials Science and Engineering, Nanjing University of Technology, Nanjing 210009, People's Republic of China
e-mail: lyanbao@163.com; ybli@njut.edu.cn

D. Li
e-mail: dongxuli@njut.edu.cn

1 Introduction

Recently, silicate-based bioactive materials have been intensively researched due to their advantages over conventional materials in a broad range of applications [1]. These bioactive materials have an ability to chemically bond to living bone through a stable apatite layer in a biological environment [2]. The presence of silanol and hydrated silica would be the prerequisite for the formation and nucleation of the apatite [3]. As compared to the traditional melt-quenching technique, new synthetic techniques, which include the sol–gel method using an evaporation-induced self-assembly (EISA) process, can adjust material properties such as surface area, ordered mesoporous structure, tunable pore size and volume [4]. Generally, EISA process starts with a homogeneous solution of soluble silica and surfactant prepared in ethanol/water solvent with $c_o \ll$ cmc, the evaporation of ethanol concentrates the depositing film in water and nonvolatile surfactant and silica species. The progressively increasing surfactant concentration drives self-assembly of silica-surfactant micelles and their further organization into liquid-crystalline mesophases [5–7]. After nucleation and orientation, mesophases developed into highly oriented mesostructures with respect to the substrate surface [8, 9]. Through variation of the initial alcohol/water/surfactant mole ratio it is possible to obtain different final mesostructures [10]. For example, Zhao and his co-workers [11–14] prepared mesoporous bioactive glasses (MBGs) with hexagonally ordered mesopores using ionic or non-ionic surfactant templates. This MBG was used to immobilize proteins or drugs with molecule sizes ranging from 2 to 30 nm [15]. Yan et al. [13] synthesized a series of highly ordered MBGs with various CaO contents and observed higher apatite formation rate with increasing CaO content.

Vallet-Regi and co-workers [16] confirmed that the addition of a small amount of P_2O_5 (~4 mol%) into bioactive glass promotes the nucleation of apatite on its surface in simulated body fluid (SBF).

In the $CaO–SiO_2–P_2O_5$ system, MBGs with higher than 10 mol% P_2O_5 content may possess the potential for higher bioactivity [6, 10]. However, to the best of our knowledge, few researchers have reported to synthesize material in this composition range or taken into account the influence of P_2O_5 content on the physiochemical properties of mesopores and the subsequent in vitro bioactivity of MBGs in SBF.

Here, we reported to prepare the novel MBGs with P_2O_5 content ranging from 10 to 30 mol%. SAXRD, N_2 sorption/desorption, TEM, FTIR and NMR techniques were employed to investigate the physiochemical properties of the mesopores and the structure of the bioglasses.

2 Experimental

2.1 Materials

Tetraethyl orthosilicate (TEOS, 98%), triethyl phosphate (TEP, 99%), calcium nitrate [$Ca(NO_3)_2{\cdot}4H_2O$, 99%], ethyl alcohol (EtOH, 99.7%), hydrochloric acid (HCl, 36–38%) were supplied by Sinopharm Chemical Reagent Co. Ltd.(China). Triblock copolymer $EO_{20}–PO_{70}–EO_{20}$ (P123, $M_w = 5650$) was purchased from Well Reagent Co. Ltd. (Nanjing, China). All chemicals were reagent grade and were used as received without further purification.

2.2 Synthesis of materials

A series of ternary $CaO–P_2O_5–SiO_2$ MBGs with different chemical compositions were prepared as listed in Table 1. Using sample P10 (10 mol% P_2O_5, 75 mol% SiO_2, 15 mol% CaO) as an example, 4 g P123 was dissolved in 60 g ethanol (EtOH), and then 1.09 g triethyl phosphate (TEP), 4.68 g tetraethyl orthosilicate (TEOS), 1.06 g calcium nitrate, and 1 g 1 M hydrochloric acid were added into P123–EtOH solution in order. The mixture was kept at room temperature for 1 day with magnetic stirring. The weight ratio of P123:ethanol:HCl (0.5 M) is 4:60:1. The as-derived clear sol was transferred into a Petri dish for gelation at 40°C for 2 days. The EISA self assembly occurs during this time using the surfactant as a template. This is followed by the process of aging at 60°C for 3 days, after which the as-prepared gels were calcined at 550°C for 5 h with a heating rate of 2°C min^{-1} in air to remove the template.

In our experiments, the molar fraction of Ca with respect to the total molar amount of Si, Ca, and P in MBGs was fixed at 15 mol% and those of Si and P were varied in different samples. MBG samples were named according to the molar fraction of P_2O_5 content (Table 1).

2.3 Characterization

Structural characterization was carried out using small angle X-ray diffractometry (SAXRD; Philips-X'pert MPD 3040) with CuK_α ($\lambda = 1.5418$ Å) radiation (40 kV, 40 mA) and transmission electron microscope (TEM, JEM-2010 UHR, Japan) at an accelerating voltage of 200 kV. FTIR spectra were collected on a Nicolet Nexus 670 Fourier transform infrared spectrometer with KBr pellet method. All NMR solid state NMR spectra were recorded on a wide bore Bruker Avance400D spectrometer at 20°C. ^{29}Si MAS NMR experiments were carried out at a Larmor frequency of 39.7 MHz and spinning speed of 4.5 kHz in a 4 mm rotor using the Hahn-echo pulse sequence with the p/2 pulse of 5.25 and 76.5 ms echo delays. ^{29}Si NMR was set up using a 3 min recycle delay. The 1.5 ppm peak of tetrakis (trimethylsilyl) methane was used for reference in ^{29}Si NMR. ^{31}P MAS NMR spectra were acquired at 81.0 MHz in the 4 mm rotor spinning at 4.5 kHz. 64 transients of a single pulse experiment with 2.5 ms p/2 pulse and 49 s recycle delay were collected for each sample. ^{31}P chemical shift was referenced to the signal of 85% H_3PO_4.

2.4 In vitro assays

The in vitro bioactivity of the MBG samples was evaluated in simulated body fluid (SBF) as described by Kokubo et al. [17]. The ionic concentrations (mM) in SBF solution were nearly equal to those in human blood plasma (Na^+: 142.0, K^+: 5.0, Ca^{2+}:2.5, Mg^{2+}: 1.5, Cl^-: 147.8,

Table 1 Chemical compositions and the amounts of reactants of different samples

Denoted samples	Molar ratio of Si:Ca:P	TEOS (g)	TEP (g)	$CaNO_3{\cdot}4H_2O$ (g)	P123 (g)	HCl (g)	C_2H_5OH (g)
P10	75:15:10	4.68	1.09	1.06	4	1	60
P20	65:15:20	4.06	2.18	1.06	4	1	60
P30	55:15:30	3.43	3.28	1.06	4	1	60

HCO_3^-: 4.2, HPO_4^{2-}: 1.0, SO_4^{2-}:0.5). The solution was buffered at pH 7.40 with tris(hydroxymethyl) aminomethane $[(HOCH_2)_3CNH_2]$ and HCl. Each specimen (0.1 g) was immersed in 100 ml SBF solution in a polyethylene (PP) bottle covered with a tight lid. The PP bottles were placed in a shaking incubator with a constant speed of 160 r min^{-1} at 37°C for 2 days. After soaking, the powders were collected by filtration, rinsed with acetone and dried in air. The powders were then evaluated by XRD, FTIR and SEM analyses to determine the mineral phase of the deposits.

3 Results and discussion

3.1 Textural properties of MBGs

Mesostructural properties of powder MBGs were evaluated by SAXRD (Fig. 1), TEM (Fig. 2) and N_2 sorption/desorption characterizations (Fig. 3). Before calcination, all samples show no diffraction peak in the small angle regime (Fig. 1a), which suggests the absence of ordered mesopores in the as-prepared MBGs; while after calcination, sample P10 (Fig. 1b) exhibits two diffraction peaks at around $2\theta = 0.85°$ and 1.28°, which can be indexed to the (100) and (110) diffractions of a two-dimensional hexagonal mesostructure. As the P_2O_5 content increases to 20%, a single diffraction peak at around $2\theta = 1.25°$ appears. As for sample P30, no significant change takes place during calcinations. These phenomena indicate that the increase of the P/Si ratio in MBGs reduces the ordering of mesostructure due to the partial collapse of the structure and/or order of the mesopores during the EISA process and calcinations. It may be ascribed to the double bond in the PO_4 polyhedron that is responsible for an imbalanced chemical interaction between the precursor and surfactant during MBG formation, resulting in the mesoporous network would be easily destroyed during calcination.

Another possibility is that ionic diffusion may account for the partial collapse of the mesoporous framework. The bond energies of Ca–O, P–O and Si–O are 322, 597 and 798 kJ/mol, respectively [18]. Higher bond energy leads to lower diffusion rate at the same temperature, and the difference between ionic diffusion rates in a glassy network may cause the collapse of glassy network and the destruction of mesopores. This may be what is occurring in sample P30, which has the highest P_2O_5 content. This places an upper limit on the P_2O_5 content ($\sim$20 mol%) that can be utilized to synthesize the well ordered MBGs using the EISA process.

The ordered mesopore of MBGs is further confirmed by TEM images (Fig. 2). TEM image of sample P10 (Fig. 2a) shows a two-dimensional hexagonal mesostructure. The MBG surface contains the mesoporous domains with the [100] zone axis oriented parallel to the electron beam. Hexagonal mesostructure can also be roughly identified in sample P20 (Fig. 2b). But for sample P30 (Fig. 2c), the mesoporous structure tends to be more disordered, which confirms the partial collapse of the mesoporous framework, inferred from the SAXRD results.

N_2 sorption/desorption isotherms and pore size distribution curves are shown in Fig. 3. Structural parameters of the different samples calculated from Fig. 3 are listed in Table 2. All the three samples exhibit a type IV isotherm with type H1 hysteresis loop, which are characteristic of independent cylindrical slim pore channels with narrow pore size distribution. As calculated from the linear part of the BET plot, the surface areas of all samples varied in the range of 370–430 m^2/g depending on the chemical composition. The single point adsorption total volumes at $P/P_0 = 0.975$ are between 0.4 and 0.5 cm^3/g. This is ascribed to the heterogeneity of conventional sol–gel-derived bioactive glasses. Especially, as shown in Fig. 3b, all samples presented a narrow pore size distribution, and the Barret–Joyner–Halenda (BJH) adsorption average pore size of samples P10, P20 and P30 are around 40 Å.

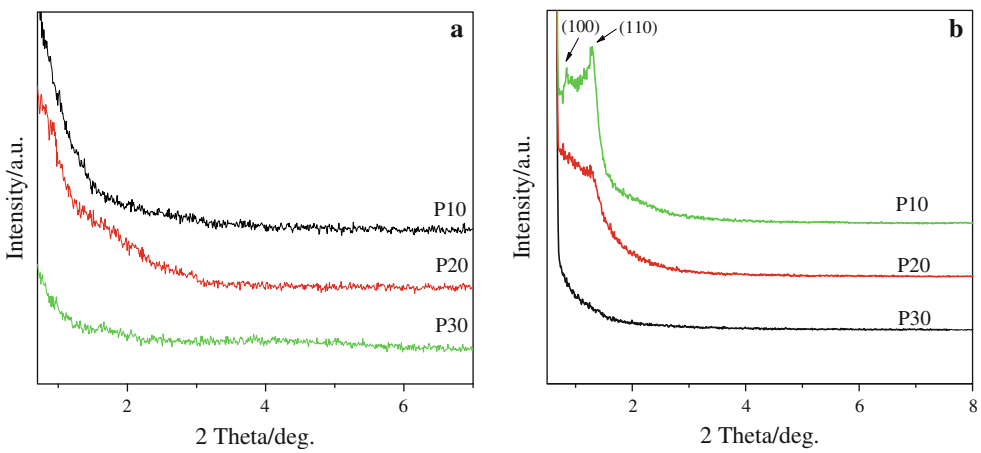

Fig. 1 SAXRD patterns of MBGs with different chemical compositions before (**a**) and after (**b**) calcinations

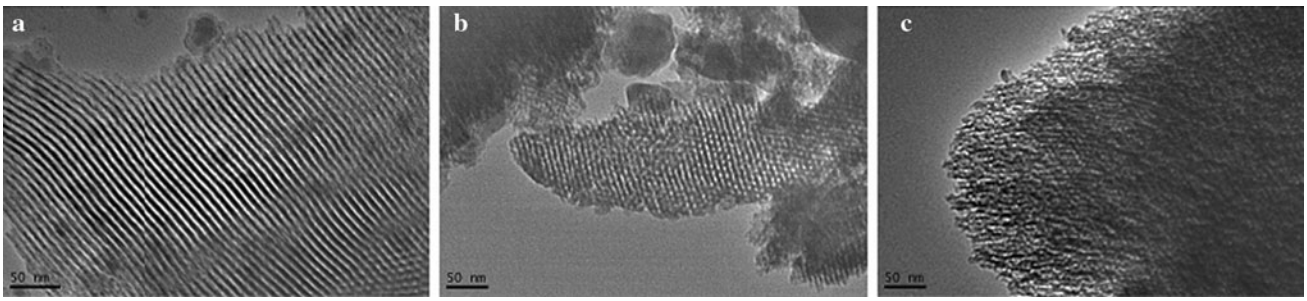

Fig. 2 TEM images of MBGs with different chemical compositions: (**a**) P10, (**b**) P20 and (**c**) P30

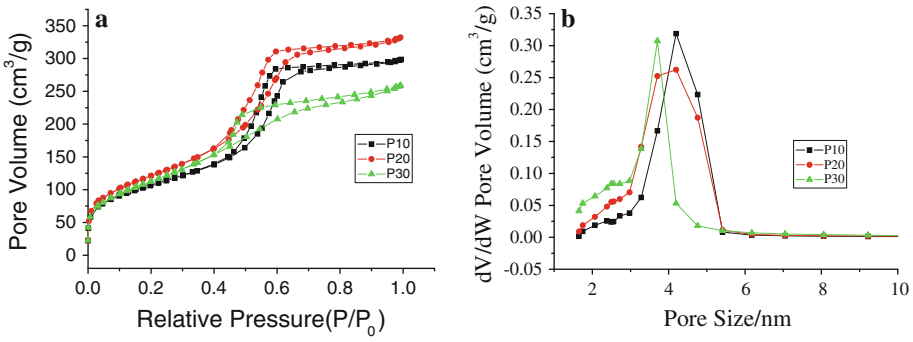

Fig. 3 N_2 sorption/desorption isotherms (**a**) and pore size distribution curves (**b**) of MBGs with different chemical compositions

^{29}Si and ^{31}P MAS NMR spectra (Fig. 4) were used to determine the bonding of the glass network and degree of condensation with the increase of P_2O_5 content. Three major peaks in ^{29}Si NMR spectra (Fig. 4a) are Q^2 (at −85 ppm), Q^3 (at −102 ppm), Q^4 (at −110 ppm) [Q^2, Q^3 and Q^4 represent the type of $(SiO)_2$=Si=$(OH)_2$, $(SiO)_3 \equiv$ Si–OH and $(SiO)_3 \equiv$ Si–O–Si, respectively] [19]. ^{29}Si MAS NMR spectra display a less condensed cross-linked structure with more silanol (–OH) groups in MBGs with the increase of P_2O_5 content. The Q^3/Q^4 ratio represents the extent of silanol condensation, indicating a more condensed framework for sample P30 than sample P10. The ^{31}P MAS NMR spectra (Fig. 4b) show two groups of signals around 0 and −11 ppm that could be assigned to Q^0 and Q^1 peaks, where Q^0 stands for phosphate units (PO_4) not bonding to silicon and Q^1 means phosphate units (PO_4) bonding to one silicon atom through one P–O–Si bond [20]. No other peaks are observed due to the absence of P atom which bonds to more than one Si atom. A small displacement of Q^0 band at 5 ppm in ^{31}P MAS NMR spectra (Fig. 4b) seems consistent with glass compositions (Table 1), leading to a distinctly disordered chemical environment [21]. The relative intensities between both signals give a Q^0/Q^1 M ratio = 1:2, which indicates that about 66% of the P atoms bond to the silica framework. ^{31}P MAS NMR spectra also indicate the glasses with high P_2O_5 content have more orthophosphate groups in isolated crystalline nano-regions. The presence of orthophosphate groups in isolated crystalline nano-regions promotes a microstructure with areas where the chemical connection of the glass structure is weaker [22]. These areas can be the preferential sites for the chemical attack during the SBF immersion.

Table 2 Structural parameters of the samples with different composition

Samples	S_{BET} (m^2/g)	V_p (cm^3/g)	D_p (Å)
P10	376	0.46	42
P20	430	0.51	42
P30	407	0.39	37

Note: S_{BET} is the BET surface area, V_p is the total pore volume, D_p is pore diameter calculated by the BJH method

3.2 In vitro bioactivity of MBGs

XRD patterns of the MBGs with different chemical compositions after soaked in SBF solution at 37°C for 3 days are shown in Fig. 5. The presence of a broad peak around $2\theta = 23°$ is due to the amorphous nature of bioglass walls. Noticeably, for sample P10, a single diffraction peak at $2\theta = 32°$ appear in the XRD pattern (Fig. 5), which can be assigned to the (211) diffraction of crystalline apatite phase. Another maximum peak in sample P20, corresponding to (002) at $2\theta = 26°$, becomes sharper and more intensive, and the (112) peak becomes sharper in sample P30. The other apatite diffraction peaks indexed to (002), (212), (213), (004), (323), and (513) also become evident. This implies that the crystallinity of the apatite precipitates

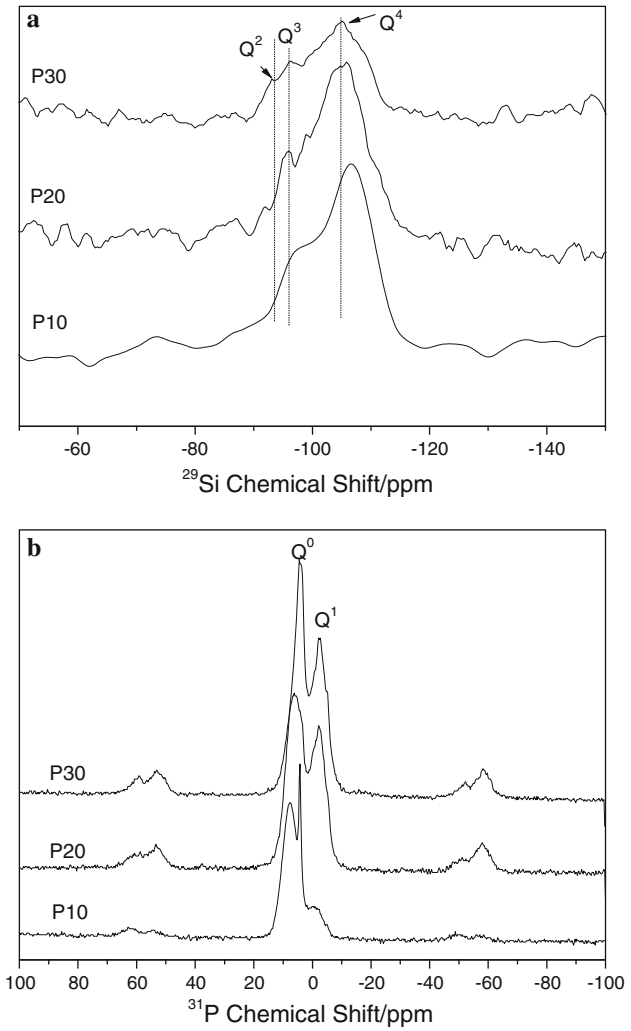

Fig. 4 ^{29}Si (**a**) and ^{31}P (**b**) MAS NMR spectra of MBGs with different chemical compositions

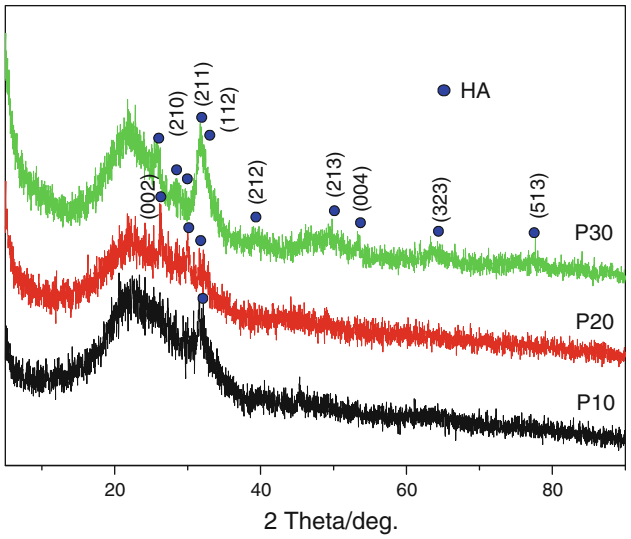

Fig. 5 XRD patterns of the MBGs with different chemical compositions after soaked in SBF solution for 3 days

increases with increasing P_2O_5 content from 10 to 30 mol%.

The FTIR spectra of the MBG surface after soaked in SBF for different times are shown in Fig. 6. For all sample, after immersion in SBF for 12 h, a strong absorption appears at 562 cm^{-1}, corresponding to the v_4 phosphate group [23]. This band became higher and sharper after the samples were soaked in SBF for longer time. The double peaks of P–O vibration mode at 562 and 602 cm^{-1} are observed after immersion in SBF for 3 days, which confirms the deposition of apatite on the MBG surface.

The variation of Ca, P and Si concentrations in the SBF after various soaking times are shown in Fig. 7. Only after immersion for 4 h, an increase of Ca and P concentrations was observed in all samples. Simultaneously, during the first 4 h, the pH value in SBF solution increases from 7.40 to 7.75 for all the three samples, which shows the rapid exchange of Ca^{2+} with H^+ or H_3O^+ from the SBF solution [2]. The increase in P concentration could be the release of P from MBGs after immersion in SBF. In the soaking interval between 4 h and 3 days, Ca and P concentrations decrease with longer soaking time, as they are consumed by the formation of apatite. The maximum release amount of Ca in sample P30 is lower than that in sample P10. This can be explained by more disordered mesopores caused by increasing P_2O_5 content, which could impede the exchange of Ca^{2+} with H^+ through mesopores and subsequent the formation rate of apatite on the glass surface. All samples show an increase of silicon concentration during the soaking period (Fig. 7c). This indicates that silicon continues to leach from the glass through the mesoporous structure, as the network breaks down. Therefore, the leaching of soluble silicon is an indicator of the degradation of MBGs [18]. The remaining calcium phosphate forms an apatite structure that is ultimately consumed in vivo during the bone growth and remodeling process [24].

Surface morphologies of MBGs before and after soaked in SBF are shown in Fig. 8. Before soaking, all MBGs show smooth and homogeneous surface [Fig. 8(a1–c1)]. After immersion in SBF for 1 day, a layer of numerous elongated particles appear, and irregular small holes are exclusively observed on the surface of P30 [Fig. 8(c2)], which means superior degradation of sample P30 in such short time. After 2 days, a rod-like morphology is observed on the surface of all samples; for sample P10 [Fig. 8(a3)], the rod-like apatite crystals are mixed with plate-like apatite with thin edges oriented perpendicular to the glass surface and distributed densely over the whole surfaces, similar to the morphology of apatite in human bone. After immersion for 3 days, a layer composed of rod-like and plate-like particles become more apparent and denser on

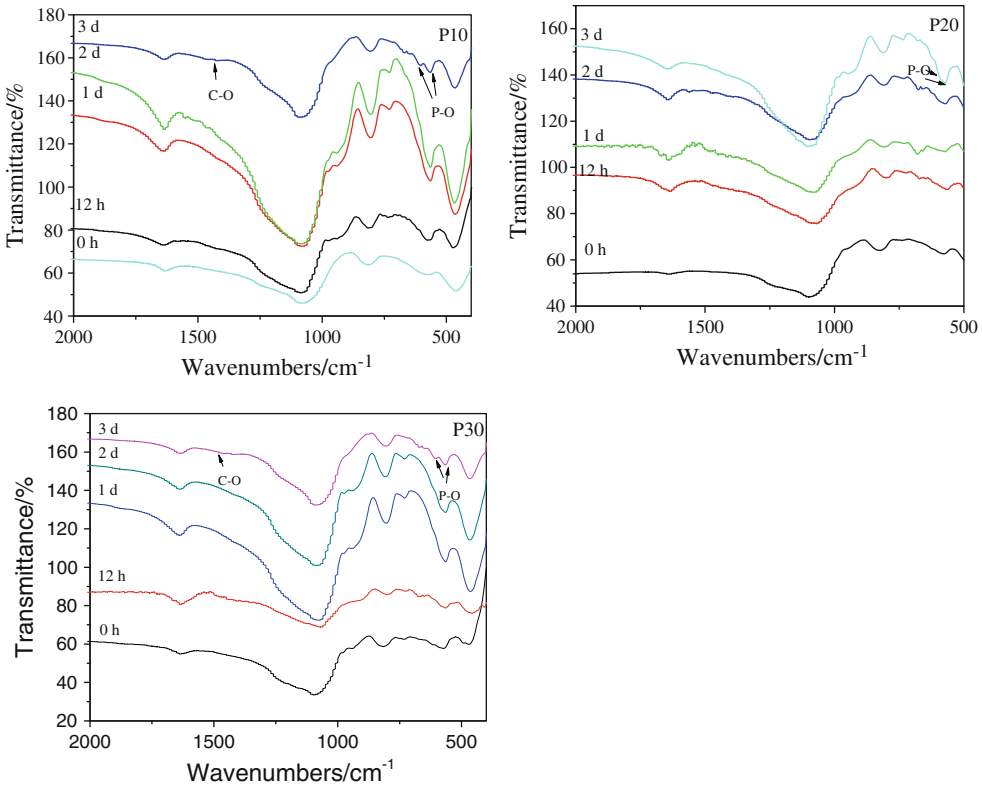

Fig. 6 FTIR spectra of MBGs with different chemical compositions after immersion in SBF solution for different times

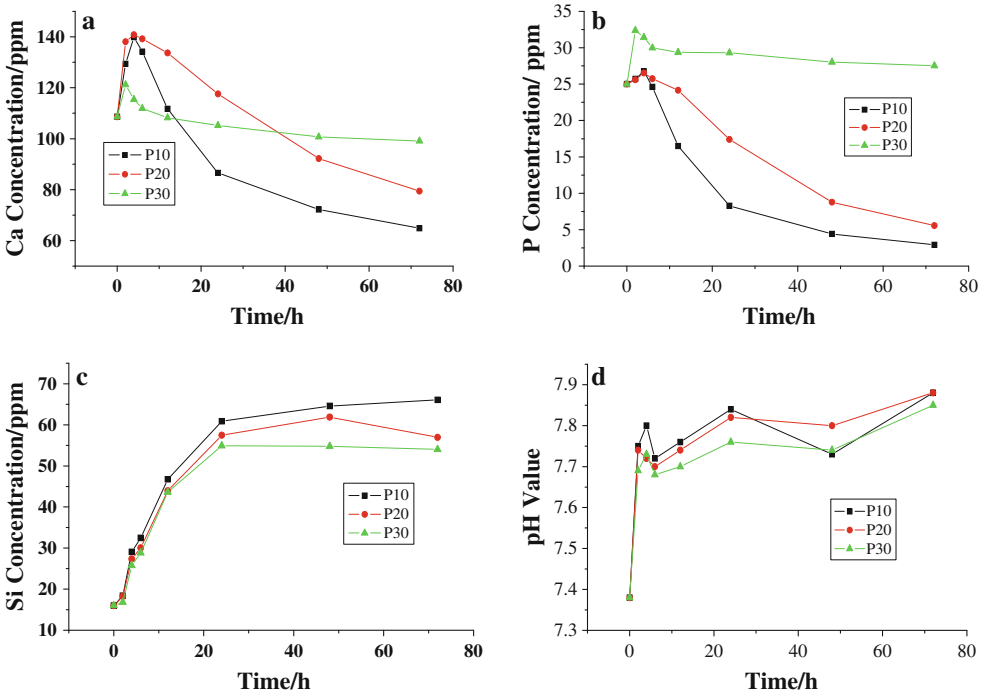

Fig. 7 Ca (**a**), P (**b**) and Si (**c**) concentrations and pH values (**d**) of MBGs with different chemical compositions after soaked in SBF for different times

the surface of all MBG samples, and more holes were detected on the surface of all samples. It is also noted that high P_2O_5 content would impede the formation of apatite after soaking in SBF for 1 day, due to the inhibited ionic exchange on the glass surface, in agreement with the ICP results shown in Fig. 7a. After 2 days, for sample P10 [Fig. 8(a3)], the predominate plate-like morphology is 6 μm in length. The dimension of formed rod-like crystals is diminished to 2 μm for sample P30 [Fig. 8(c3)]. After 3 days, plate-like aggregates in sample P30 become more

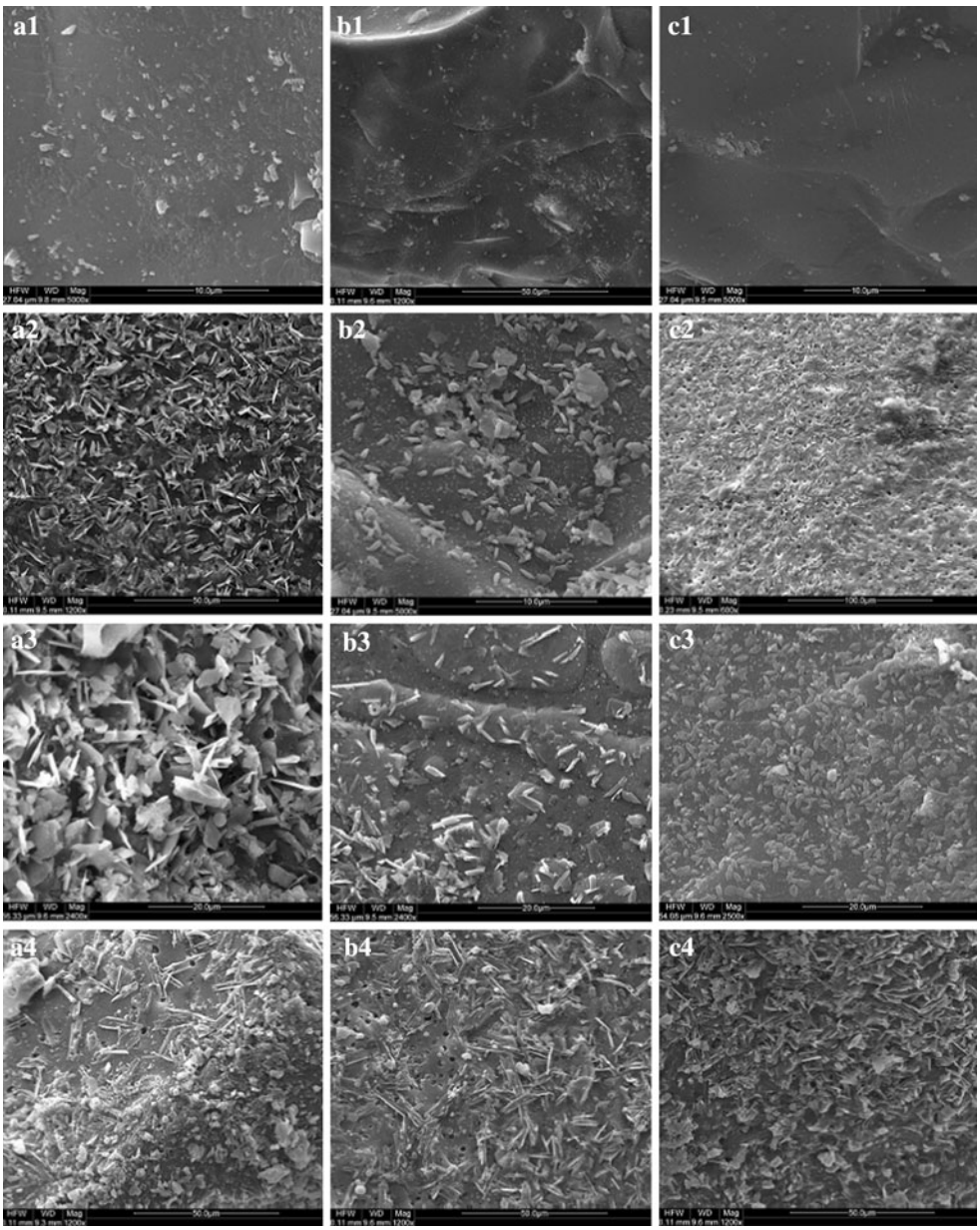

Fig. 8 SEM images of the MBGs with different chemical compositions (**a**, **b**, **c** stands for sample P10, P20, P30) before (**1**) and after soaked in SBF for 1 day (**2**), 2 days (**3**) and 3 days (**4**), respectively

apparent and denser than those in other two samples [Fig. 8(c4)].

4 Conclusion

Mesoporous bioactive glasses (MBGs) with different P_2O_5 contents (10, 20, and 30 mol%) were successfully synthesized using EO_{20}–PO_{70}–EO_{20} (P123) as template by a combination of the sol–gel method and EISA. The reduction and broadening of the peak in the small angle regime with increase of P/Si ratio places an upper limit on the P_2O_5 content ($\sim$20 mol%) that can be employed to prepare the ordered MBGs through the EISA process. This may be ascribed to the double bond in PO_4 polyhedron and different ionic diffusion which together account for partial collapse of mesoporous network. ^{29}Si NMR spectra indicates a more condensed framework for P30 than P10 and ^{31}P NMR spectra indicates the glasses with high P_2O_5 content have more orthophosphate groups in isolated crystalline nano-regions which makes better bioactivity during the SBF immersion. ICP, XRD and

FTIR results after 3 days of in vitro assay confirm more apparent and denser plate-like apatites on the surface of P30. Besides, all samples show an increase of silicon concentration during certain soaking period from ICP results, showing the degradation of MBGs in SBF solution.

Acknowledgments This work was supported by National Natural Science Foundation of China (No. 50802042), Natural Science Foundation of Jiangsu province (No. BK2008379) and the State Key Laboratory of Materials-Oriented Chemical Engineering (KL09-6).

References

1. Zhao DY, Huo QS, Feng JL, Chmelka BF, Stucky GD. Nonionic triblock and star diblock copolymer and oligomeric surfactant syntheses of highly ordered, hydrothermally stable, mesoporous silica structures. J Am Chem Soc. 1998;120(24):6024–36.
2. Horcajada P, Ramila A, Boulahya K, Gonzalez-Calbet J, Vallet-Regi M. Bioactivity in ordered mesoporous materials. Solid State Sci. 2004;6(11):1295–300. doi:10.1016/j.solidstatesciences.2004.07.026.
3. Li PJ, Ohtsuki C, Kokubo T, Nakanishi K, Soga N, Nakamura T, et al. Apatite formation induced by silica-gel in a simulated body-fluid. J Am Ceram Soc. 1992;75(8):2094–7.
4. Kresge CT, Leonowicz ME, Roth WJ, Vartuli JC, Beck JS. Ordered mesoporous molecular-sieves synthesized by a liquid-crystal template mechanism. Nature. 1992;359(6397):710–2.
5. Lu Y, Ganguli R, Drewien C, Anderson M, Brinker C, et al. Continuous formation of supported cubic and hexagonal mesoporous films by sol–gel dip-coating. Nature. 1997;389:364–8.
6. Bruinsma PJ, Kim AY, Liu J, Baskaran S. Mesoporous silica synthesized by solvent evaporation: spun fibers and spray-dried hollow spheres. Chem Mater. 1997;9(11):2507–12.
7. Ogawa M. Formation of novel oriented transparent films of layered silica-surfactant nanocomposites. J Am Chem Soc. 1994;116(17):7941–2.
8. Yang H, Coombs N, Sokolov I, Ozin GA. Morphogenesis of shapes and surface patterns in mesoporous silica. Nature. 1996;381:589–92.
9. Aksay I, Trau M, Manne S, Honma I, et al. Biomimetic pathways for assembling inorganic thin films. Science. 1996;273:892–8.
10. Brinker CJ, Lu YF, Sellinger A, Fan H. Evaporation-induced self-assembly: nanostructures made easy. Adv Mater. 1999;11(7):7579–85.
11. Yu CZ, Fan J, Tian BZ, Zhao DY, Stucky GD. High-yield synthesis of periodic mesoporous silica rods and their replication to mesoporous carbon rods. Adv Mater. 2002;14(23):1742–5.
12. Yan XX, Yu CZ, Zhou XF, Tang JW, Zhao DY. Highly ordered mesoporous bioactive glasses with superior in vitro bone-forming bioactivities. Angew Chem Int Ed. 2004;43(44):5980–4. doi:10.1002/anie.200460598.
13. Yan XX, Huang XH, Yu CZ, Deng HX, Wang Y, Zhang ZD, et al. The in vitro bioactivity of mesoporous bioactive glasses. Biomaterials. 2006;27(18):3396–403. doi:10.1016/j.biomaterials.2006.01.043.
14. Yan XX, Deng HX, Huang XH, Lu GQ, Qiao SZ, Zhao DY, et al. Mesoporous bioactive glasses. I. Synthesis and structural characterization. J Non-Cryst Solids. 2005;351(40-42):3209. doi:10.1016/j.jnoncrysol.2005.08.024.
15. Zhao LZ, Yan XX, Zhou XF, Zhou L, Wang HN, Tang HW, et al. Mesoporous bioactive glasses for controlled drug release. Microporous Mesoporous Mater. 2008;109(1-3):210–5. doi:10.1016/j.micromeso.2007.04.041.
16. Salinas AJ, Vallet-Regi M, Izquierdo-Barba I. Biomimetic apatite deposition on calcium silicate gel glasses. J Sol-Gel Sci Technol. 2001;21(1–2):13–25.
17. Kokubo T, Takadama H. How useful is SBF in predicting in vivo bone bioactivity? Biomaterials. 2006;27(15):2907–15. doi:10.1016/j.biomaterials.2006.01.017.
18. Braun M, Hartmann P, Jana C. F-19 and P-31 NMR-spectroscopy of calcium apatites. J Mater Sci Mater Med. 1995;6(3):150–4.
19. Lippmaa E, Magi M, Samoson A, Engelhardt G, Grimmer AR. Structural studies of silicates by solid-state high-resolution Si-29 NMR. J Am Chem Soc. 1980;102(15):4889–93.
20. Szu SP, Klein LC, Greenblatt M. Effect of precursors on the structure of phosphosilicate gels—Si-29 and P-31 MAS NMR-study. J Non-Cryst Solids. 1992;143(1):21–30.
21. Aguiar H, Solla EL, Serra J, Gonzalez P, Leon B, Almeida N, et al. Orthophosphate nanostructures in SiO_2–P_2O_5–CaO–Na_2O–MgO bioactive glasses. J Non-Cryst Solids. 2008;354(34):4075–80. doi:10.1016/j.jnoncryso1.2008.05.031.
22. Brauer DS, Karpukhina N, Law RV, Hill RG. Structure of fluoride-containing bioactive glasses. J Mater Chem. 2009;19(31):5629–36. doi:10.1039/b900956f.
23. Fowler BO. Infrared studies of apatites. I. Vibrational assignments for calcium, strontium, and barium hydroxyapatites utilizing isotopic substitution. Inorg Chem. 1974;13(1):194–207. doi:10.1021/ic50131a039.
24. Greenspan DC, Zhong JP, Wheeler DL. Bioactivity and biodegradability: melt vs. sol–gel derived bioglass in vitro and in vivo. Bioceramics. 1998;11:345–8.